

Flux Modulation from Non-Axisymmetric Structures in Accretion Discs

Peggy Varnière & Eric G. Blackman^a

^a*Department of Physics and Astronomy and Laboratory for Laser Energetics,
University of Rochester, Rochester NY, 14627*

Abstract

Non-axisymmetric accretion discs can lead to flux variability. Here we provide an analytic framework for modeling non-axisymmetric structures like hotspots and spiral waves and their influence on observed timing measurements. The presently unexplained Low-frequency Quasi-Periodic Oscillations (LFQPO), observed in X-ray binaries and cataclysmic variables, could be the result of such discs. Our framework serves as a guide to quantify the properties that non-axisymmetric structures produced by nonlinear accretion disc models must have in order to explain observed features such as LFQPOs. The results from our microquasar applications also provide analogous predictions for X-ray modulation in active galactic nuclei. The formalism and physical interpretation is of practical use for generic non-axisymmetric accretion disc systems.

Key words: accretion, accretion discs, X-rays: binaries, galaxies: active

PACS: 97.10.G, 97.80, 98.62.M

1 Introduction

X-ray emission from accreting black holes in binary stellar systems varies on time scales ranging from milliseconds to years. Variability on time scales longer than days appears to be driven by changes in the accretion rate onto the black hole, and is often manifested as transient outbursts in which the luminosity of a source changes by a million-fold Lasota (2001). At the shortest time scales, quasi-periodic oscillations (QPOs) are observed in the X-ray emission. The highest frequency QPOs ($> 100\text{Hz}$) are consistent with those expected from general relativistic orbits near the innermost stable orbit around the black hole, and they are likely caused by inhomogeneities in the inner accretion flow (Remillard et al., 2002, Stella & Vietri, 1998). However, the cause of low frequency QPO (LFQPO)s 0.1–20 Hz is still a mystery. This motivates

the work herein. For neutron star X-ray binaries, low frequency QPOs can be sub-divided into more precise categories (e.g. Psaltis et al., 1999). Here we focus on a basic paradigm for the modulation and leave explanations of possible harmonic relations and phase lag behavior Varnière (2005) for further work. Black hole microquasars avoid the role of any solid stellar surface, and offer a purer probe of the accretion process without interaction with a stellar surface. The basic properties of LFQPOs that any model needs to explain are these:

(1) LFQPOs often appear to be present in widely spaced observations, over a period of weeks, with fractionally narrow frequency widths ($\Delta\nu/\nu \approx 1/30$) (Morgan et al., 1997, Remillard et al., 1999). Although the observations are not continuous, the fact that the LFQPO are observed to be the same (within a very small variation) over several observations within the same week/month, suggest that the QPO are likely always present during that time, at least when averaged over such long time scales within the hard state; there are periods where the LFQPO appear and disappear on timescale of a few seconds. If LFQPOs result from inhomogeneities orbiting at a Keplerian speed in the accretion disc they are constrained to a narrow range of radii.

(2) LFQPO amplitudes are typically 5-10% RMS (root mean squared), but can reach 20% RMS. Given that the X-ray luminosities of black hole binaries approach 10^{39} erg s⁻¹, LFQPOs involve an enormously energetic fraction of the accretion flow.

(3) On the other hand, LFQPOs are transient features, so the spectral properties of the X-ray emission when LFQPOs are present and absent can be used to constrain the LFQPO origin (Muno et al., 1999, Sobczak et al., 2000).

(4) The 0.1–20 Hz LFQPOs only appear when the non-thermal component of the X-ray spectrum is strong, and their fractional amplitudes increase with energy between 2–20 keV. However, a thermal component that contributes $\sim 10\%$ of the X-ray emission at lower energies must also be present, and the frequencies of the LFQPO appear to be correlated best with this. The energy output of accreting black holes can generally be decomposed into a ~ 1 keV thermal component (thought to originate from the optically thick accretion disc) and a non-thermal component with a power-law spectrum extending beyond 100 keV (thought to result from inverse-Compton scattering of cool photons by a corona of hot electrons.) Thus, it appears that the 0.1–20 Hz QPOs either originate in the boundary between the disc and the corona, or are part of the mechanism which accelerates the hot Comptonizing electrons.

As mentioned, LFQPOs can be further subdivided (Psaltis et al., 1999), but the above represents a basic set of characteristics that a zeroth order LFQPO flux modulation model should explain.

Two different conceptual paradigms for LFQPOs have been proposed in this regard: (1) In the centrifugal pressure supported boundary layer model (CENBOL, Chakrabarti & Manickam, 2000), a QPO is produced by a shock in the accretion flow where it makes a transition from a Keplerian disc to a hot Comptonizing region. If the cooling time of the post-shock region is resonant with the free-fall time at the shock, the shock can oscillate radially with a frequency on order a Hz. The QPO is, in principle, produced because the shock modulates the flux of seed photons that reach the Comptonizing post-shock region. In this model, the LFQPO would represent a global radial oscillation that modifies the emitted flux. (2) A second paradigm for LFQPOs is non-axisymmetric structures in the disk. Their motion around the black hole would lead to flux modulation. These structures could move at the Keplerian speed, a precession speed (such as Lense-Thirring) or a phase velocity associated with a structural instability. One example occurs in the accretion-ejection instability model (AEI, Tagger & Pellat, 1999, Varnière & Tagger, 2002). Here a spiral shock forms in an accretion disc threaded by a vertical magnetic field. The dispersion relation is similar to that of a galactic disc but with the gravitational potential replaced by a magnetic one. At the co-rotation radius, at which the Keplerian velocity matches that of the pattern, a Rossby vortex forms and emits vertical Alfvén waves into a corona. The LFQPO would result from the orbit of this non-axisymmetric structure in the disc. 2D numerical simulations of this instability, for example, demonstrated (Varnière *et al.*, 2003) that the X-ray flux was modulated. However, in 2D, the constraints on the cause of the modulation and how it can be stronger and weaker were limited.

In this paper, we focus on the paradigm exemplified by the latter type of model, namely the production of LFQPOs by the orbit of a non-axisymmetric structure. Here we do not focus on the specific origin of the structure but rather investigate the consequences of the presence of such a structure. We investigate the specific question of whether a stable pattern in an accretion disc can reproduce the observed characteristics of LFQPO simply by its motion around the central engine. In Sec. 2 we give analytical formulae that can be used to model arbitrarily shaped blobs and spirals as non-axisymmetric disc features. In Sec. 3 we compute the emission from an accretion disc with such non-axisymmetric structures and discuss the influence of the shape of the particular non-axisymmetric structures on the RMS LFQPO amplitude. We also discuss the parameter choices which provide the most observationally consistent non-axisymmetric structures for the microquasar example discussed above. We also note that the formalism is generically applicable to other non-axisymmetric accretion disc systems. We conclude in Sec. 5.

2 Modeling non-axisymmetric discs

Blobs and spirals are two useful categories of non-axisymmetric structures. We use blob to indicate a generic localized feature and spirals to indicate the more specifically identifiable global structure produced by gravitational or MHD instabilities—the latter via the accretion-ejection instability (AEI) i.e. Tagger & Pellat 1999. Here we do not detail the formation of these non-axisymmetric structures but focus on providing an analytic framework that characterizes their shape for practical use and allows observational implications for flux modulation to be quantified.

Because discs of observed systems such as microquasars and active galactic nuclei (AGN) are not resolved, the disc structure cannot be directly imaged. But from studying the timing evolution of the flux, especially the presence of the LFQPO with its frequency and RMS amplitude, we can infer what structures might be present. We concentrate on the RMS amplitude of the modulation, assuming that the frequency is already matched by the presumed location of the given structure.

Taking into account the disc thickness is a particularly important aspect of our endeavor. For discs viewed at highly inclined angles, the shadowing from a local thickening of the disc can be important. The height and temperature profiles are coupled in the hydrostatic equilibrium approximation. Although we make this approximation here, detailed 3D simulations will ultimately be needed to get an exact profile of h and T for a more realistic disc.

2.1 Analytic expression for the disc thickness

For the disc thickness, we write

$$h(r, \phi) = h_o(r) + h_1(r(\phi), \phi) = h_o(r) + s(r - r_s)d(r) \quad (1)$$

where h_1 is a perturbation in thickness around the unperturbed thickness h_o , r is the radial location, and ϕ is the azimuthal angle. We have used $h_1 = s(r - r_s)d(r)$, where s is a “shape” function. The latter is finite only near the disc structure causing the non-axisymmetry. The blob or spiral wave feature is localized by $r_s \equiv r_c e^{\alpha(r)\phi}$, where r_c is the point where the structure begins and α is the opening angle of the structure. The quantity $d(r)$ is a thickness function which is defined as the height of the disc at each point.

We now take $s(r - r_s)$ to be a Gaussian and d to be a power-law in r . This provides a simple but useful framework to model non-axisymmetric structures.

From (1) we then have

$$h(r, \phi) = h_o(r) + \tilde{\gamma} \left(\frac{r_c}{r} \right)^\beta e^{-0.5 \left(\frac{r-r_s}{\delta} \right)^2}, \quad (2)$$

where the constant β measures how fast the thickness decreases from the maximum, δ parameterizes the radial extent of the structure, and $\tilde{\gamma}$ defines the disc thickness at r_c . We allow the maximum height $\tilde{\gamma}$ to be a function of the unperturbed thickness at that point, that is $\tilde{\gamma} = \gamma h_o(r_c)$. This allows consideration of cases with similar h_o/r but different r_c . We also consider the number of times the non-axisymmetric structure winds around the disc.

The influence of the parameters in (2) is illustrated in Fig. 1. The role of α is seen in Fig. 1a which shows a top view of two spirals' "spines" (i.e. the line defined by $r_s(\alpha, \phi, r_c)$ tracing the maximal height above the unperturbed disc at each ϕ). The larger the α the more open the spiral. The role of parameters $\tilde{\gamma}$, δ , and β are seen in Fig. 1b which shows cross sections of the disc height profile for different ϕ projected into the r, z plane for $r_c = 1.5$. Increasing δ would increase the full width-half-maximum of the peaks, which in practice has a larger effect on the rise to the peak than the fall because the Gaussian perturbation is superimposed upon a positively sloped disk. Increasing $\tilde{\gamma}$ would increase the maximum height above the h_o , and the downward slope of the line that connects the peaks at different ϕ values would be steeper for larger β . Fig. 1c shows a 3-D close-up of the inner region of the disc with a one-armed spiral characterized by $h_o/r = 0.01$, $r_c = 3$, $\alpha = 0.07$, $\tilde{\gamma} = 0.3$, $\beta = 2$, and $\delta = 0.2$ at an viewing angle of 70° from the normal.

2.2 Emission

Having obtained an expression for the disc height, we compute the temperature using the approximation that $c_s = h\Omega$, which gives $T = \mu/R_{gas}c_s^2$. This means, for example, that a change in temperature by 20% is related to a change in thickness of about 45%.

In order to determine the observational effect of a non-axisymmetric disc thickness, we compute the flux as a function of azimuth that an observer would received as time-dependent flux modulation when the disc rotates. Assuming that the spectrum from each point is a blackbody, we use the height-temperature relation above to compute the photon flux

$$f(E) = \frac{2}{c^2 h^3} \frac{E^2}{\exp[E/kT] - 1}. \quad (3)$$

We then sum the flux from each cell, multiply by $\cos([\pi/2 - \theta] - \zeta)$, where θ is the disc inclination angle from the normal and

$$\zeta = \text{atan} \left(\frac{dh}{dr} \cos \phi - \frac{dh}{rd\phi} \sin \phi \right). \quad (4)$$

We trace rays from the individual cells to the observer in order to determine whether the flux is intercepted by the outer portions of the disc. We compute the observed spectrum as the structure rotates by viewing a single snapshot at all angles ϕ . The spectrum is taken as multi-temperature blackbody, and we sum the number of photons received. We compute the Fourier transform of the profile in order to estimate the amplitudes of any modulation at multiples of the pattern frequency.

Our simple spectral modeling does not include scattering in the disc atmosphere, the presence of an electron corona, or special and general relativistic (GR) effects in part because the LFQPOs observed in microquasars could be coming from shadowing by structures at > 100 gravitational radii. Also, the non-relativistic formalism applies at all radii for generic disks systems around stars. We note however, that non-Keplerian origins of the non-axisymmetries leading to LFQPOs are also possible, such as binary induced precession, spiral wave phase velocities that differ from Keplerian, or Lense-Thirring precession. The latter is an intrinsically general relativistic phenomenon. While relativistic effects should be considered in future more detailed applications to compact systems, here we focus on qualifying the effect of the key parameters in (2) on the modulation, not on the particular source of the the non-axisymmetry.

3 Simulated flux modulation

Table 1 shows a subset of our numerically solved cases for the blob and spiral. Cases 1-15 can be considered spirals, whilst cases 16-19 can be considered blobs because their structures extend less than 2π radians. For all cases we have taken an inclination angle of 70° , motivated by the inferred observation angle of GRS 1915+105 (Mirabel & Rodriguez, 1994).

There is degeneracy in the relative influences of the various parameters of (2) on the RMS amplitude of modulation of Table 1, but it is instructive to discuss the influence of each of the parameters separately.

3.1 Spirals and physical interpretation of the geometric parameters

First notice the lack of influence of the range of $\phi > 2\pi$ in Table 1: For each ϕ , most of the modulation comes from the most inward “bump” in $h(r)$. Allowing for more than 1 bump does not modify the RMS modulation significantly, as seen in cases #1, #2, #3. For the majority of the other cases we will therefore consider only the range of $\phi \leq 2\pi$.

The parameter $\tilde{\gamma}$, measures the maximum thickness of the perturbation. Its effect is evident in comparing cases #3, #6, #7. The greater $\tilde{\gamma}$, all else being equal, the stronger the modulation. This is because a thicker structure more strongly shadows the inner disc. A change in thickness of 70% means a temperature change of $\sim 50\%$. This somewhat extreme case is taken to illustrate the role of $\tilde{\gamma}$ on the RMS amplitude. Constraining the amplitude modulation from first principles requires a 3D MHD disc simulation that exhibits a spiral wave instability. Here the non-axisymmetry would emerge rather than be imposed. Previous 2.5-D (i.e. no dynamical vertical structure) disc simulations unstable to the AEI exhibit spiral waves, and lead to a temperature variation typically of order of 20 – 30% in the hydrostatic equilibrium approximation (Varnière et al, 2003). But in 3-D, hydrostatic equilibrium would underestimate the perturbation thickness of an AEI generated spiral because of additional heating from spiral shock dissipation. Thus a higher $\tilde{\gamma}$ than that obtained from the 2.5D simulation can be expected, provided the AEI survives in 3-D.

Because $\tilde{\gamma} \equiv \gamma h_o(r_c)$ is the maximum height of the spiral arm, a change in h_o (the zeroth order disc thickness) also increases the modulation. By comparing cases #14 and #15 we see that changing h_o by a factor of two is not exactly the same as changing $\tilde{\gamma}$ by a factor of two because increasing $\tilde{\gamma}$ also increases the difference between the maximum height of the perturbation and h_o .

As discussed at the end of Sec. 2, the parameter β measures how fast the maximum height along the spiral decreases with radius. Its effect is revealed in cases #3, #4, #5. The RMS amplitude of the modulation increases with β for an $\alpha > 0$ spiral. A rapidly decreasing height perturbation with radius means that the height also rapidly decreases along the spiral. This causes a stronger modulation by producing a stronger azimuthal variation. This is particularly important for tight spirals (small $\alpha \sim 0.05$): were it not for a large β , little non-axisymmetry would otherwise arise.

The simulations relevant for studying the influence of r_c , the initial radius where the perturbation begins (r_c), are #6, #9, #10 and #11. We see a maximum in the RMS amplitude for r_c around $2 r_{in}$, where r_{in} is the inner disc radius: When the spiral is too near r_{in} , it obscures less of the inner disc which is the most luminous part. On the other hand, if the spiral is too far out,

it can only obscure a less luminous outer region giving a smaller modulation. The combination of these effects is an intermediate r_c for maximal modulation. Since the position of the spiral is chosen based on the LFQPO frequency, a correlation between the RMS amplitude and the frequency of the QPO is expected. In practice this may be hard to disentangle from variations in the other parameters.

The influence of the parameter α , which determines the opening of the spiral wave can be seen from simulations #6, #12 and #13. There we see that the more open the spiral, the higher the RMS amplitude. This is because a more open spiral means a more non-axisymmetric thickness profile, leading to a higher RMS amplitude of modulation.

Finally, consider the parameter δ , which measures the width of the spiral or blob at its base. From cases #6 and #8 we see that a larger δ , implies a larger RMS amplitude. For our choice of a highly inclined system, this trend results because a larger δ makes more of the region inner to the peak of the perturbation more perpendicular to the line of sight. This produces a larger observed flux when the observer is looking at the disk from an azimuth for which the line of sight intersects the inner part of the perturbation. But as the disk rotates, the outer edge of the perturbation comes into view, and the shadowing of the inner region occurs similarly for large or small δ . The contrast in flux (and thus the RMS amplitude of the modulation) is thus larger for larger δ , explaining the trend.

3.2 Blobs or hot spots

Because the difference between spirals and blobs in our model is just whether the structure extends for a range of $\phi \geq 2\pi$ (spiral) or $\phi < 2\pi$ (blob), the parameter influences are similar for the two cases. The relevant blob simulations are #16, #17, #18, and #19. There we see that a blob can create a non-negligible modulation of the X-ray flux but to reach a large RMS amplitude, the blob needs a large azimuthal extent—making it more banana or spiral shaped. The reason is that a localized structure does not provide much shadowing over a disc rotation period and thus offers only a weak RMS modulation. In contrast to spirals, such blobs probably cannot account for observed LFQPOs in microquasars.

4 Expected dependence of RMS amplitude on inclination and energy

Because the modulation comes from shadowing, the disc inclination angle θ is important in determining the maximum shadowing and thus the maximum RMS amplitude that a given choice of parameters can produce. Motivated by a comparison with the LFQPOs of GRS1915+105 (see *e.g.* the review McClintock & Remillard 2004), we again focus on the parameter choices of simulation #8 and vary the inclination angle to obtain different values of the RMS amplitude. Fig. 5 shows the result. As expected, the more edge-on the view, the higher the RMS amplitude. Present observational data are insufficient to definitively confirm or contradict the predicted behavior. Such a trend could explain the **extremely weak** LFQPO in Cyg X-1, as the RMS amplitude expected from the inferred inclination angle is very small¹. More objects with a wider range of inclination angles are needed. Additional techniques of determining the disc inclination angle in microquasars besides using the jet propagation direction would also be desirable. In the case of neutron stars, data from eclipsing binaries and dippers provides good information on the binary and thus disk inclinations (e.g Frank et al., 1987).

It is important to note that the dependence of the rms amplitude on the inclination angle shown in Fig. 5 is displayed only for the case in which all other parameters are identical. Therefore the trend shown should be seen inside the same “family” of objects—those having similar disk properties. It was shown in table 1 that some parameters can have a greater influence on the rms amplitude than the inclination. These parameters could give rise to low inclination source with a strong spiral having a higher rms amplitude than a high inclination source with a very small spiral

Using the relation between T and h , we can also study how the RMS amplitude behaves as function of energy. Several studies show that LFQPO amplitudes rise with energy up to 15-20keV, although the behaviour at higher energies seems to depend on the source, for example in GRS 1915+105 (Tomsick & Kaaret, 2001). We have not included a corona (high energy component) in our simple spectral modeling herein, but we can make a qualitative prediction of the LFQPO amplitude vs. energy trend by studying the RMS amplitude as function of our predicted disc flux, supplemented by knowledge of the disc/corona flux ratio taken from observation. We find that the RMS amplitude of the modulation gets bigger at higher energy. This is simply because a spiral with $r_c/r_{in} \sim 2$ is hotter than the surrounding disc and therefore its blackbody contribution to the spectrum peaks at a higher temperature.

¹ Cyg X-1 seems to show a weaker and broader structure than the “usual” LFQPO that could be a weak LFQPO in agreement with this simple model.

When a corona is present, this trend would apply at low energies, but we expect a critical energy above which the corona strongly dominates and the trend reverses.

We emphasize that in order to predict the exact position of the modification in the trend at high energies, we need to take into account not only the disk but also the corona self-consistently. This is beyond the scope of the present paper which is intended to show the basics of how flux can be modulated by non-axisymmetric structures.

5 Summary and Discussion

We have presented a simple analytical framework for modeling and interpreting how non-axisymmetric disk features such as spirals or blobs can create modulation of the observed flux from an accretion disk. We connect the disk geometry to the flux via the hydrostatic equilibrium assumption. Our focus on spirals is motivated by their production in disc simulations of the AEI and the efficacy with which such spirals seem to account for the observed LFQPO properties of microquasars, see *e.g.* the review McClintock & Remillard, 2004. Our formalism does not depend on the origin of the non-axisymmetric structures. Rather, it is used to quantify the influence of a range of generic spirals and hotspot geometries.

Using our formalism (with parameters guided by a fit to the LFQPO properties of GRS1915+105) we expect that the RMS amplitude increases with disc inclination because the modulation from a spiral or blob results from shadowing of the inner disc. Because the spiral is the hottest part of the disc for typical $r_c \sim 2r_{in}$, we also find that the RMS amplitude should increase with energy, except above energies where the emission becomes strongly corona dominated. More quantitative modeling and more observations are needed.

If the time scale of a LFQPO in a black holes system is indeed determined by an orbit or pattern speed of a non-axisymmetric feature, then at a given number of gravitational radii, the LFQPO frequency should scale inversely with the black hole mass. If accretion disks around AGN and microquasars incur similar instabilities, then a 1 – 10Hz LFQPO in microquasars would correspond to a $< 10^{-6}$ Hz LFQPO in AGN. Testing this prediction is presently difficult because it pushes the present limits of continuous observation times for individual AGN.

Finally note that although we have focused on black hole systems because of the LFQPO observations in microquasars, the analytic formalism for modeling the influence of spirals and hot spots herein does not depend on the compact-

ness of the central object. It can also be applied to discs around neutron stars, white dwarfs, or young stellar objects.

More work is needed to incorporate our basic framework into detailed models of individual LFQPO sourcecs.

Acknowledgments: We acknowledge support from NSF grant AST-0406799 and NASA grant ATP04-0000-0016. PV thanks M. Tagger for discussions and we thank M. Munro for discussions and allowing use of some code.

References

- [1] Caunt, S. E. & Tagger, M. 2001, *A&A*, 367, 1095
- [2] Chakrabarti, S. K., & Manickam, S. G. 2000, *ApJ*, 531, L41
- [3] Frank, J., King, A. R., & Lasota, J.-P. 1987, *A & A*, 178, 137
- [4] Hartnoll, S. A. & Blackman, E. G. 2002, *MNRAS*, 332, L1
- [5] Hartnoll, S. A. & Blackman, E. G. 2000, *MNRAS*, 317, 880
- [6] Homan, J., Wijnands, R., van der Klis, M., Belloni, T., van Paradijs, J., Klein-Wolt, M., Fender, R., & Méndez, M. 2001, *ApJS*, 132, 377
- [7] Lasota, J.-P. 2001, *New Astronomy Reviews*, 45, 449
- [8] Mirabel, I.F. & Rodriguez L.F., 1994., *Nature*, 371:4648.
- [9] Molteni, D, Sponholz, H., & Chakrabarti, S. K. 1996, *ApJ*, 457, 805
- [10] Morgan, E. H., Remillard, R. A., & Greiner, J. 1997, *ApJ*, 482, 993
- [11] Munro, M. P., Morgan, E. H., & Remillard, R. A. 1999, *ApJ*, 527, 321
- [12] Nowak, M. & Wagoner, R.V., 1991, *ApJ*, **378**, 659.
- [13] Nowak, M. & Wagoner, R.V., 1992, *ApJ*, **392**, 697.
- [14] Masset, F., 2000, *A&A*, **141**, 165-173.
- [15] McClintock, J.E. & Remillard, R.A., Chapter 4 in "Compact Stellar X-ray Sources," eds. W.H.G. Lewin and M. van der Klis, Cambridge University Press.
- [16] Pacinski, B., Witta, P.J., *A&A*, **88**, 23.
- [17] Psaltis, D, Belloni, T. & van der Klis, M., 1999, *ApJ* **520**, 262.
- [18] Remillard, R. A., Munro, M. P., McClintock, J. E., Orosz, J. A. 2002, *ApJ*, 580, 1030

- [19] Remillard, R. A., Morgan, E. H., McClintock, J. E., Bailyn, C. D., & Orosz, J. A. 1999, ApJ, 522, 397
- [20] Rodriguez, J., Varnière, P., Tagger. M., and Durouchoux, P., 2002, A&A, **387**, 487-496.
- [21] Sobczak, G. J., McClintock, J. E., Remillard, R. A., Cui, W., Levine, A. M., Morgan, E. H., Orosz, J. A., & Bailyn, C. D. 2000, ApJ, 544, 993
- [22] Stella, L. & Vietri, M. 1998, ApJ, 492, L59
- [23] Stehle,R., Spruit, H.C., MNRAS, 1999, **304**, 674-686.
- [24] Tagger, M., 1999, Proc of the 5th Compton Symp. Porthsmouth (USA), AIP COnf. Proc., **510**, 129. ([astro-ph/9910365](#))
- [25] Tagger, M., and Pellat, R., 1999, A&A, **349**, 1003 (**TP99**)
- [26] Tagger, M., Henriksen, R.N., Sygnet, J.F. and Pellat, R., 1990, ApJ **353**, 654.
- [27] Tagger, M., Varnière, P., Rodriguez, J., and Pellat, R., 2004, ApJ, **607**,410-419.
- [28] Tomsick, J.A. and Kaaret, P., 2001, ApJ, **548**, 401.
- [29] Varnière, P.,, 2005, A&A, **434**, L5.
- [30] Varnière, P., Rodriguez, J. and Tagger. M., 2002, A&A, **387**, 497-506.
- [31] Varnière, P. and Tagger. M., 2002, A&A, **394**, 329-338.
- [32] Varnière, P., Munro, M., Tagger. M., 2003, SF2A procceding, [astro-ph/astro-ph/0310026](#).

| # | h_o/r | r_c/r_{in} | α | β | γ | δ | angular extend | rms |
|------|---------|--------------|----------|---------|----------|----------|----------------|-------|
| # 1 | 0.01 | 2. | 0.05 | 0.5 | 1 | 0.1 | 6π | 2.3% |
| # 2 | 0.01 | 2. | 0.05 | 0.5 | 1 | 0.1 | 4π | 2.2% |
| # 3 | 0.01 | 2. | 0.05 | 0.5 | 1 | 0.1 | 2π | 2.2% |
| # 4 | 0.01 | 2. | 0.05 | 0.3 | 1 | 0.1 | 2π | 0.9% |
| # 5 | 0.01 | 2. | 0.05 | 0.7 | 1 | 0.1 | 2π | 3.7% |
| # 6 | 0.01 | 2. | 0.05 | 0.5 | 2 | 0.1 | 2π | 4.3% |
| # 7 | 0.01 | 2. | 0.05 | 0.5 | 3 | 0.1 | 2π | 7.3% |
| # 8 | 0.01 | 2. | 0.05 | 0.5 | 2 | 0.2 | 2π | 5.6% |
| # 9 | 0.01 | 1.5 | 0.05 | 0.5 | 2 | 0.1 | 2π | 3.5% |
| # 10 | 0.01 | 2.5 | 0.05 | 0.5 | 2 | 0.1 | 2π | 3.7% |
| # 11 | 0.01 | 3. | 0.05 | 0.5 | 2 | 0.1 | 2π | 3.2% |
| # 12 | 0.01 | 2. | 0.03 | 0.5 | 2 | 0.1 | 2π | 1.7% |
| # 13 | 0.01 | 2. | 0.1 | 0.5 | 2 | 0.1 | 2π | 12.3% |
| # 14 | 0.02 | 2. | 0.05 | 0.5 | 2 | 0.1 | 2π | 8.6% |
| # 15 | 0.01 | 2. | 0.05 | 0.5 | 2 | 0.1 | 2π | 9.2% |
| # 16 | 0.01 | 2. | 0.05 | 0.5 | 2 | 0.2 | $3\pi/2$ | 5.5% |
| # 17 | 0.01 | 2. | 0.05 | 0.5 | 2 | 0.2 | π | 4.7% |
| # 18 | 0.01 | 2. | 0.05 | 0.5 | 2 | 0.2 | $\pi/2$ | 3.0% |
| # 19 | 0.01 | 2. | 0.05 | 0.5 | 2 | 0.2 | $\pi/4$ | 1.6% |

Table 1

For each simulation, all parameters, and the resulting RMS amplitude are given. The inclination angle for all cases is 70° , which is the value for GRS1915+105 inferred from the orientation of the disk (Mirabel & Rodríguez 1994), assuming the jet is perpendicular to the jet. The angular extend of the spiral/blob is given in fraction of 2π .

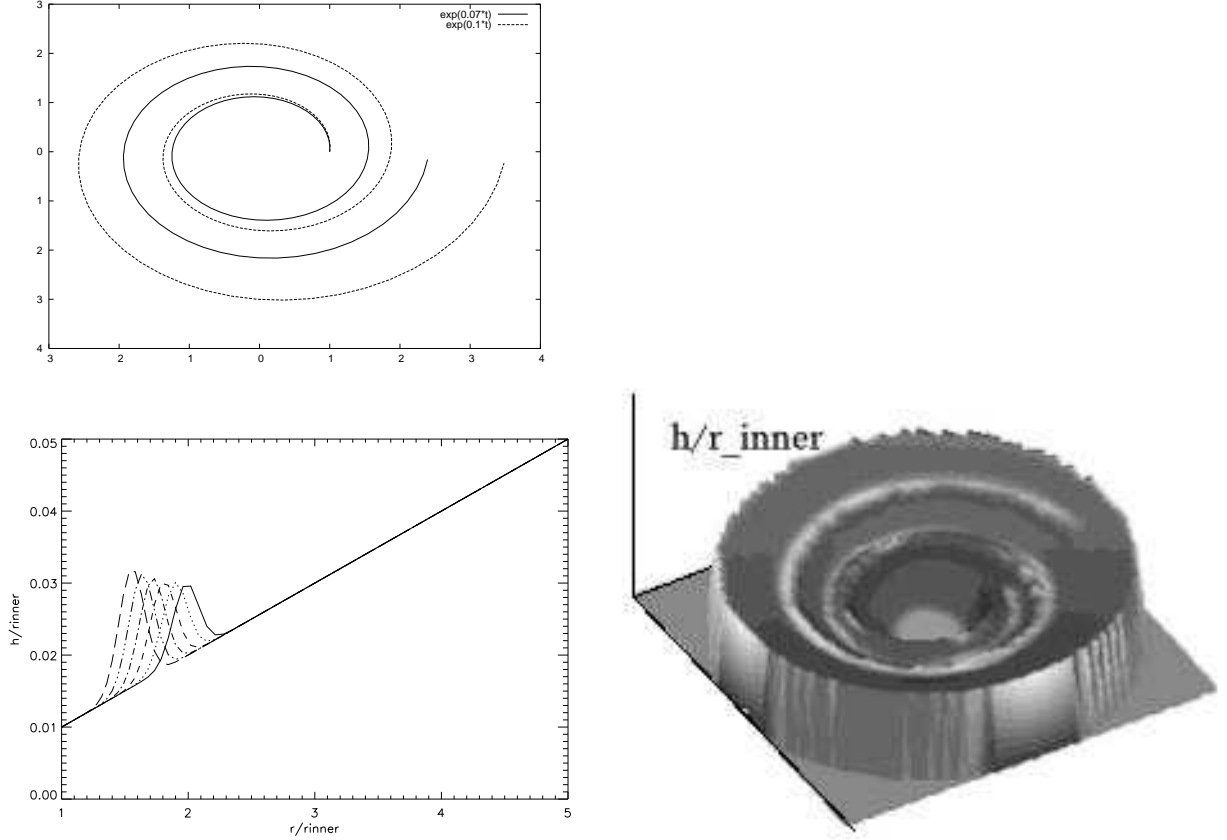


Fig. 1. (a) Schematic top view of of spiral spines (line tracing the peak in height of the spiral) for two different choices of α . (b) Schematic slices of the disc height profile for an example spiral as a function of radius for $h_o/r = 0.01$. Profiles at different azimuths are all projected into the same $r - z$ plane. The peak in the left-most curve occurs at r_c . The width of the curves is determined by the parameter δ . The downward slope of the line connecting the peaks is determined by β (for a fixed α) and the maximum height of the peaks is determined by $\tilde{\gamma}$ (see text). (c) 3-D close up of the inner part of the disc with the spiral wave, the viewing angle is 70° with $h_o/r = 0.01$, $r_c = 3$, $\alpha = 0.07$, $\gamma = 0.3$, $\beta = 2$, $\delta = 0.2$.

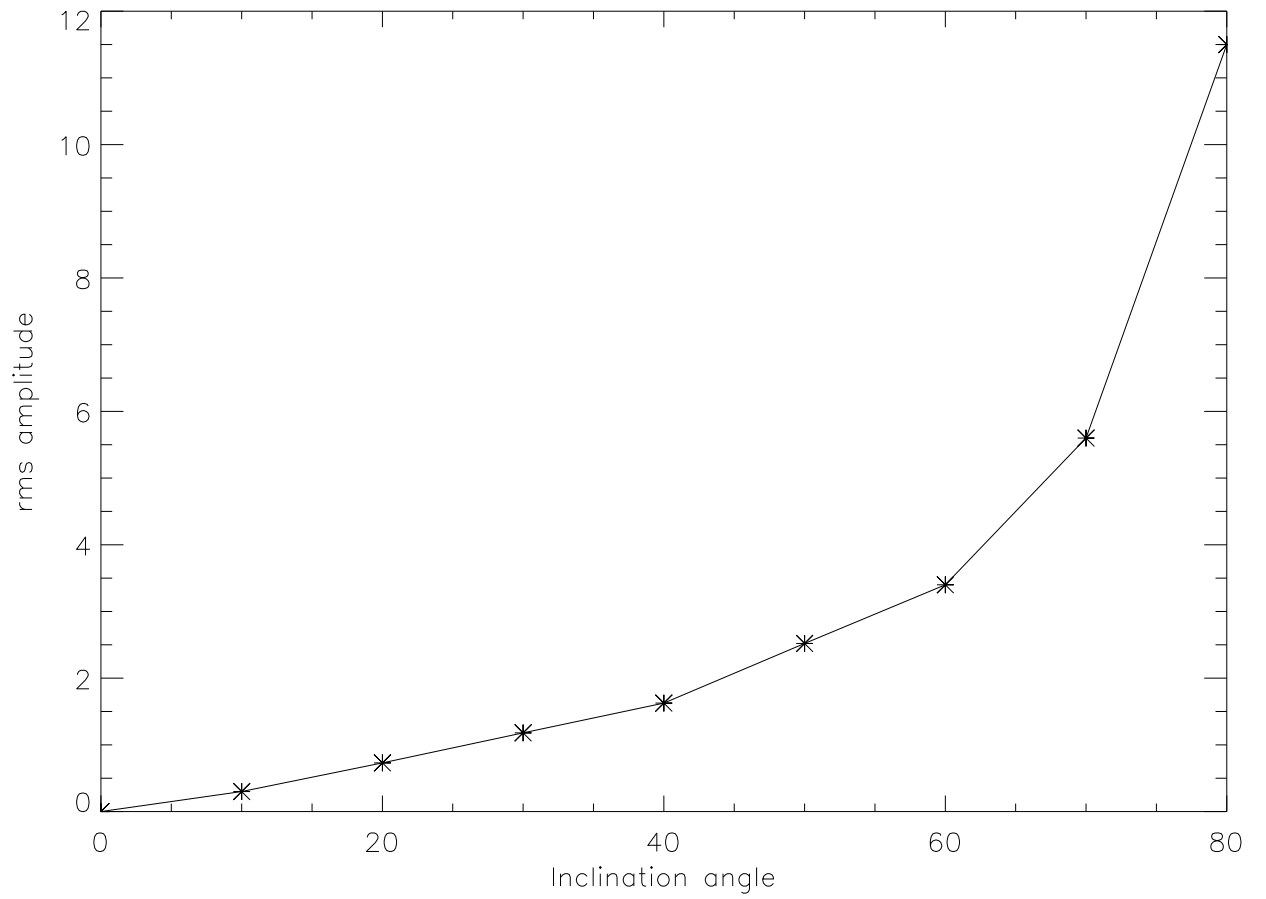


Fig. 2. Evolution of the RMS as a function of the inclination angle θ for the simulation case #8 of Table 1.